# Pattern formation of underwater sand ripples with a skewed drive

F. Bundgaard,* C. Ellegaard,† and K. Scheibye-Knudsen
*Niels Bohr Institute, Blegdamsvej 17, DK-2100 Copenhagen, Denmark*

T. Bohr
*Institute of Physics, Technical University of Denmark, Building 309, DK-2800 Kgs. Lyngby, Denmark*

T. Sams
*Danish Defence Research Establishment, Ryvangs Allé 1, P.O. Box 2715, DK-2100 Copenhagen, Denmark*

In this paper we present an experimental study of the dynamics of underwater sand ripples when a regular pattern of ripples is subjected to a skewed oscillatory flow, i.e., one not perpendicular to the direction of the ripple crests. Striking patterns with new, superposed ripples on top of the original ones occur very quickly with a characteristic angle, which is, in general, not perpendicular to the flow. A slower, more complex transition then follows, leading to the final state where the ripples are again perpendicular to the flow. We investigate the variation of the superposed pattern as a function of the direction, amplitude, and frequency of the drive, and as a function of the viscosity (by changing the temperature). We quantify the dynamics of the entire transition process and finally study the grain motion around idealized (solid) skewed ripples. This leads to a characteristic mean path of a single particle. The path has a shape close to a parallelogram, with no apparent connection to the pattern of real, superposed ripples. On the other hand, a thin layer of sand sprinkled on the solid ripples leads to qualitatively similar patterns.

## I. INTRODUCTION

When a flat bed of sand is subjected to an oscillatory water flow, regular patterns of ripples will appear almost inevitably. This phenomenon, well known from shallow-water zones like beaches, has been investigated for almost a century. Classical studies [1] show that so-called *rolling grain ripples* will form initially, when the sand bed becomes linearly unstable. However, these small, moving filaments of grains are always transient and will develop into the stable, triangular *vortex ripples* perpendicular to the water flow. Vortex ripples are named so because of the vortex with reversed flow created behind the ripple crest in each half period of the oscillation. The slope of the sides is roughly at the angle of repose of the sand, while the ripple distance $\lambda$ from one crest to the next is set by the amplitude $a$ of the water motion. $\lambda$ is roughly independent of the frequency $f$ [2–4], but scales linearly with the driving amplitude so that $\lambda \approx 1.3a$.

Recent studies of vortex ripples have investigated and modeled the flow, shear stress, and sediment transport on the ripples in one dimension [5–8]. The more general pattern forming properties [9] of two-dimensional sand beds have been subject to studies [4,10,11], which have focused on the dynamics of the pattern when the driving parameters are changed. In these studies a fully developed bed of vortex

sand ripples was subjected to a change in the driving amplitude and frequency, and secondary instabilities, some of which are intrinsically two dimensional, were found. Thus, if a bed of perfectly periodic ripples is driven with a larger amplitude than the one used for creating the system, it will be forced into a state with a larger ripple distance. This can happen with or without encountering secondary instabilities, as stated below.

Hansen *et al.* [4] describe how a *stability balloon* exists around a given point in the $(a, f)$ plane: This means that it is possible to change the frequency and amplitude for stable perpendicular ripples within this region, without encountering secondary instabilities in the pattern formation. Thus, raising the amplitude to a point within the stability balloon will simply lead to a slow increase in $\lambda$ of the original ripples. However, when a regular pattern is subjected to a larger amplitude which lays outside the stability balloon a secondary instability will occur. One might expect, in analogy with the Rayleigh-Bénard system, that this transition would be of the Eckhaus type [9], where ripples are compressed and dilated in the direction of the drive, making the instability one dimensional. However, the intermediate states develop transverse oscillations of ripple crests, named *bulging* [4,10,11]. This bulging transition resembles the *skew-varicose* instability in the Rayleigh-Bénard system, which is believed to occur because of mean flow effects [9,12].

The occurrence of bulging transitions where significant parts of the ripples cease to be perpendicular to the drive, implies that one needs a better understanding of the properties of ripples that are skewed with respect to the drive. These properties are largely unexplored, and, as seen below, present surprising phenomena. The present work is a detailed study of the dynamics of vortex ripples when they are sub-

---

*Present address: MIC–Department of Micro and Nanotechnology, Technical University of Denmark, Building 345 East, DK-2800 Kgs. Lyngby, Denmark. Electronic address: bundgard@nbi.dk URL: www.nbi.dk/~bundgard

†Electronic address: ellegard@nbi.dk

jected to a flow at an angle different from the one that has originally formed them. We observe a complex transition from the original skewed ripples to the final perpendicular ones. The character of the intermediate states is different for small and large skewness of the ripples. If the initial ripples are close to being perpendicular to the drive, the bulging transition occurs, and the ripple crests undergo sinusoidal perturbations, but for larger skewness the deformations appear more zigzag like with straight segments in two distinct directions. Such states resemble the "brick patterns" first observed by Bagnold [1] and the "pearling transition" described in [4]. Thus, by varying the angle between the initial, unperturbed ripples and the drive, we can interpolate between transitions of "bulging" type and ones closer to "pearling."

For large skewness, a pattern of well-defined ripples superposed on the initial ones appears at a new angle which is generally not perpendicular to the drive. The angle is measured experimentally using Fourier spectra in which the emerging peaks are sharp, reflecting the regularity of the ripple pattern.

Our initial expectation was that this angle would depend strongly on the angle between the unperturbed state and the new driving direction, as well as on the driving amplitude. This was thought because these quantities characterize the geometry of the pattern and therefore the possible geometrical resonances, like Bragg scattering over sea bottom ripples [13]. However, the dependence on the initial angle was small in this regime, whereas an unexpected dependence on the frequency of the oscillatory drive was found. This suggests that the phenomenon observed is viscous rather than geometric. Studying the water motion over a fixed bed of ripples, the flow becomes independent of gravity and if the angle depends on the frequency, it can do so only through the combination of the frequency divided by the viscosity $\nu$, like the transverse instabilities in the flow around an oscillating cylinder [14]. Multiplying by either the amplitude of the drive or the initial ripple distance we get the Stokes number $St = a^2 f / \nu$. The angle of the new ripples is then a function of the Stokes number. This allows an investigation into the possible equivalence of changing the frequency and the viscosity. Experimentally, the change in viscosity was realized by changing the temperature of the water.

To understand the hydrodynamical properties of the flow, we studied trajectories of single particles as they are dragged along by the oscillating flow. Such tracks turn out to be surprisingly universal, and do not allow a determination of the angles of the pattern. On the other hand, we show that the main features of the superposed ripple patterns can be reproduced in the patterns formed by a thin layer of sand sprinkled on a plastic model of ripples (analogously to the experiments by Matsunaga and Honji [14] for the nonskew case).

Section II describes the experimental setup and the typical experimental procedure. Next, in Sec. III we show how the angle of the superposed ripples depends on the different driving parameters. This is followed by Sec. IV, where the temporal development of the transition for different driving parameters is quantified. Finally, in Sec. V A we focus on the tracking of single particles in their flow across the ripples and, in Sec. V B, on the patterns of thin layers of sand
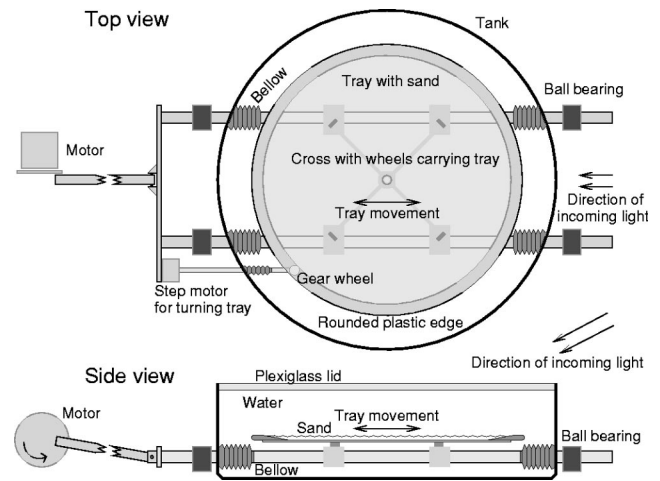


FIG. 1. The experimental setup. A circular tray with a 2 cm thick layer of sand is oscillated horizontally in a closed, water-filled tank. The tray can be turned using a step motor, so that a bed of sand ripples can be subjected to water motion at any given angle. An overhead camera records the images.

sprinkled on plastic ripples. The work presented here can be found in further detail in [15].

## II. EXPERIMENTAL SETUP

The experimental setup is similar to those used in previous experiments [4,10,11] in that a tray with sand is oscillated in stationary water. The main additional feature is that the round tray may be rotated to any angle, so that a ripple pattern created in the sand at one angle may be subjected to a new flow at a different angle.

The setup is sketched in Fig. 1. A circular tank 150 cm in diameter and 42 cm high is filled with water and covered by a Plexiglass lid. Inside, an aluminum tray 120 cm in diameter, carrying a 2 cm thick layer of sand, is oscillated horizontally. A rounded edge on the tray minimizes the vortices made when oscillating the tray and a gently inclining "beach" makes a smooth transition between the plastic edge and the layer of sand. The sand area is around 100 cm in diameter. Two steel rods connected by a cross carry the tray inside the tank. The tray is attached only in the center, while four wheels underneath the plate support it. Using a step motor outside the tank, it is possible to turn the tray accurately without opening the tank, so that a bed of sand ripples can be subjected to a water flow at any given angle.

Outside the tank, four ball bearings carry the steel rods, protruding through holes in the wall of the tank. To keep the water inside, flexible bellows molded in rubber are attached to the tank in one end and to the rod in the other.

The sand is observed from above using an 8-bit black-and-white Basler A101f FireWire camera with a resolution of $1300 \times 1300$ pixels. With a viewing field of 120 cm across (the diameter of the tray) a resolution of 1.2 mm/pixel is obtained. To make the three-dimensional ripples visible, light is directed onto the ripples from the side, at a flat angle around 30°, so that one side is illuminated, while the other
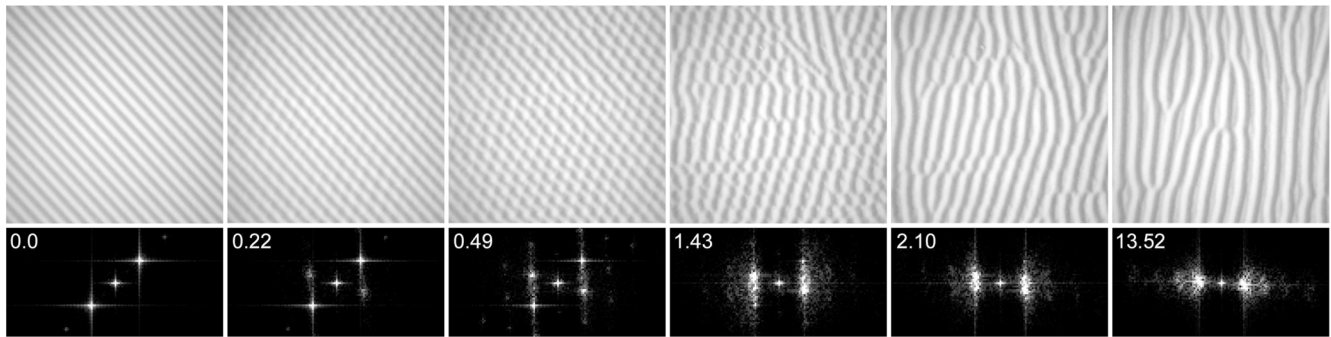
FIG. 2. The typical development of an experiment. The middle part of the tray with the defect-free pattern is shown. It is oscillated horizontally with a driving amplitude of 29 mm, a frequency of 0.92 Hz, and the initial angle set to 43°. The initial ripple distance is 30 mm. The time in minutes and seconds is shown in the corner of the Fourier transform below the pictures. In the first image the original ripples are seen, while superposed ripples emerge on the second image. The two distinct directions collapse to new ripples almost perpendicular to the driving motion, while the defects created slowly disappear by recombination or by climbing.

remains in the shade. This produces a striped image, as shown in Fig. 2.

The camera is directly connected to a photodiode triggering the camera when the tray is in a certain position. Typically a picture is captured every fifth oscillation.

We use spherical glass balls 250–350 $\mu$m in diameter and with a density $\rho$ of 2.65 g/cm$^3$ instead of natural sand, yielding a slightly lower angle of repose of the ripples. The camera resolution of 1.2 mm/pixel gives roughly 4 grain diameters per pixel.

### A. The typical experiment and data analysis

All the experiments investigating the superposed sand ripples have been performed in the same, following manner. First, the sand bed is prepared by completely leveling the surface. A grid of parallel, 15 mm high V-shaped profiles 30 mm apart is pressed into the sand and carefully pulled up again. This leaves an array of parallel grooves, perpendicular to the direction of motion. The distance between the grooves has been chosen to provide a sufficiently large number of ripples on the tray. Because of the many parameters that are varied in the system, we chose to keep the initial ripple distance constant throughout all experiments.

The Plexiglass lid is lowered onto the tank and the tray is oscillated a dozen times, transforming the middle part of the flat bed with grooves into a defect-free pattern of real vortex ripples. The driving amplitude used is 22 mm, which corresponds to the ripple distance $\lambda$ of 30 mm (recalling that $\lambda \approx 1.3a$). The frequency is set to 0.9 Hz. Only the middle part of the tray is analyzed, since the border effects near the edge influence the pattern formation, leading to various defects.

The tray is then turned to the desired angle and oscillation is started with the new amplitude and frequency. A typical development of the ripples can be seen in Fig. 2.

When a series of images has been recorded, a fast Fourier transform (FFT) is performed on the middle $512 \times 512$ pixels of each original image. It has been experimentally verified that the influence of the border effects on this area is negligible. This was done by observing the system for an extended period of time. It was seen

that the middle part of the pattern eventually became stable, even though new defects were constantly created further out because of the edge geometry.

The original ripple distance $\lambda$ and angle $\alpha$ with respect to the direction of the water motion are both set before the experiment is started, and can be extracted from the FFT along with the new ripple angle $\beta$ of the superposed ripples and the new ripple distance $\nu$, all shown in Fig. 3. Three examples of different angles $\beta$ are given in Fig. 4.

By thresholding the FFT corresponding to the images when the superposed ripples have just emerged (usually after 50 oscillations, depending on the frequency), only two distinct pairs of spots corresponding to the two directions remain. The center of mass of each of the four spots is found and the distances $2\mathbf{d}_\lambda$ and $2\mathbf{d}_\nu$ between the two pairs and the angles are calculated. The two ripple distances are found using that $\lambda = N/|\mathbf{d}|$, where $N$ is the side length of the quadratic image measured in pixels. The angles can be measured directly, as seen in Fig. 3. Changes of less than 0.1° can be detected, while the overall error in the system remains below 1°.

Figure 2 illustrates the typical development of the ripples in time. The first FFT simply shows the direction and distance of the original ripples, but already in the second image,
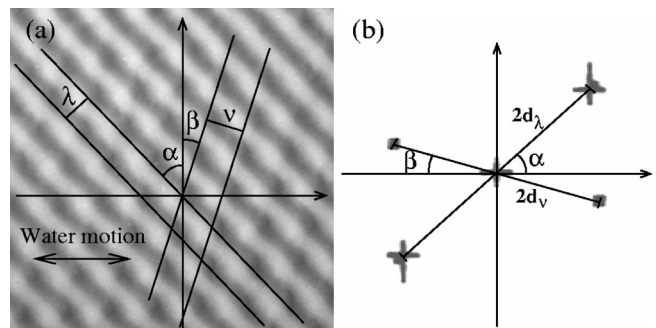


FIG. 3. (a) The initial angle $\alpha$ and the angle $\beta$ of the superposed ripples are defined on the image, taken after about 50 oscillations, and are found again on (b), the corresponding FFT. The ripple distances $\lambda$ and $\nu$ of the original and superposed ripples are inversely proportional to the distances $d_\lambda$ and $d_\nu$, measured on the FFT.
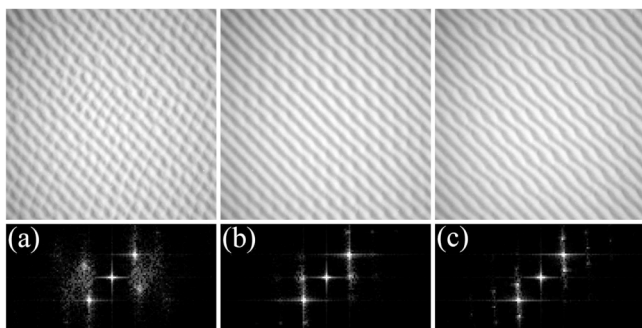
FIG. 4. Three different examples of the angle $\beta$ of the superposed ripples, with the same initial angle $\alpha=45°$. (a) Amplitude $a=26$ mm and frequency $f=0.86$ Hz giving a $\beta$ of $23°$. (b) $a=31$ mm and $f=0.73$ Hz resulting in superposed ripples almost completely perpendicular to the driving motion. (c) $a=36$ mm and $f=0.62$ Hz making new ripples at an angle $\beta$ of $-16°$. The definitions of the angles are seen in Fig. 3.

after 22 s (18 oscillations), the superposed ripples start to appear at an angle of about 15° clockwise from vertical. This is seen in the FFT as two pale spots to the left (above) and to the right (below) the central spot. In the third picture, after 49 s, the old and new ripples are equally strong and the spots in the FFT therefore appear equally bright. In the fourth picture, the two distinct ripple orientations have started to collapse, as can be seen from the FFT, where the spots are much less well defined. "Clouds" of smaller wavelengths are seen on the outside of the spots. The collapse continues in the fifth image, meaning that the defects now present in the pattern move and cancel each other out, and the system moves toward a new stable pattern perpendicular to the driving motion, with a ripple distance again corresponding to the new driving amplitude. In the last image, almost a quarter of an hour later, this new, larger ripple distance is present (seen by the spots of the FFT being closer to each other). The small pieces of ripple between the crests of the large ones can be detected in the FFT as the two small clouds furthest apart. These ripples will disappear along with most of the defects, if the oscillation is continued for a sufficient period of time. The time scale of the transition to a well-ordered, almost defect-free pattern depends on the driving parameters and ranges from hours to days. Further remarks on this will be made in Sec. IV.

### III. EXPERIMENTAL RESULTS

As stated in the Introduction, for geometrical reasons initially it was thought that the angle of the superposed ripples would predominantly depend on the angle $\alpha$ of the original ripples. Therefore, preliminary experiments were carried out so that the driving amplitude would match the distance between the ripples along the driving direction, while the frequency was set so that $af$ was kept constant. In this manner the time scale of the transition is roughly constant, meaning that the different characteristic phases of the pattern transitions occur at roughly the same points in time for all experiments.

However, contrary to the frequency independence of the ripple distance observed with the perpendicular ripples [1,2,10], the angle of the superposed ripples is affected when changing the frequency alone as well as when changing the amplitude. Furthermore, our present data suggest that the initial angle $\alpha$ influences the angle $\beta$ little, or not at all, when $\alpha$ lies between 35° and 50°.

These initial results made us focus on two ways of varying the parameters: either keeping amplitude and frequency constant while varying the initial angle $\alpha$, or keeping the initial angle constant while varying $a$ and $f$. These two approaches are described in the following two sections. Finally, because of the strong influence of the frequency on $\beta$, a series of experiments with varying temperature (and thereby viscosity, as stated in the Introduction) were conducted, but with fixed $a$, $f$, and $\alpha$. These results are presented in the last section.

Important to note is the intrinsic uncertainty which exists in the formation of these patterns, so that the same initial conditions yield different angles of the superposed ripples. A standard deviation of about 3° is found.

### A. Varying the initial angle $\alpha$

The first experiments were carried out varying the initial angle $\alpha$ only. The imprinted initial ripple distance of all our experiments is 30 mm, corresponding to a driving amplitude of 22 mm. By then changing to a driving amplitude of 30 mm and 0.80 Hz, the secondary instability bulging occurs, as seen in the leftmost image of Fig. 5. The corresponding FFT, recorded after 100 oscillations for each experiment, shows a parenthesislike structure on both sides of the two spots, corresponding to the larger and smaller ripple distances in the skewed directions of the bulges. The internal parentheses are brighter than the external ones. This corresponds to the fact that the areas of smaller ripple distance, where the ripples are compressed, are flatter and more blurred, thus giving less contrast.

When the initial ripples are no longer perpendicular to the driving motion, but tilted more than 5°–10°, the bulges become asymmetric. The half which is closest to being perpendicular to the driving motion grows. The other half of the zigzag, which has an angle larger than that of the original ripples, decreases as if being stretched between the two more perpendicular adjacent parts. The stretching makes this part of the ripple thinner. In the FFT of the image at $\alpha=15°$ this is clear: Two halves (top left and bottom right) of the internal parentheses are now much stronger than the other two, which have almost vanished, while two distinct dots further apart, at the top right and the bottom left, have emerged and correspond to the stretched part of the ripples with the smaller width.

From $\alpha=10°$ until around 35° the general picture is roughly the same: When raising $\alpha$, both the spots caused by the thick bulges and those caused by the thin connecting parts turn counterclockwise in the FFT, meaning that the zigzag turns with the initial ripples. The thin parts are stretched more and more, when the angle is increased, as seen in Fig. 5 at 30°.
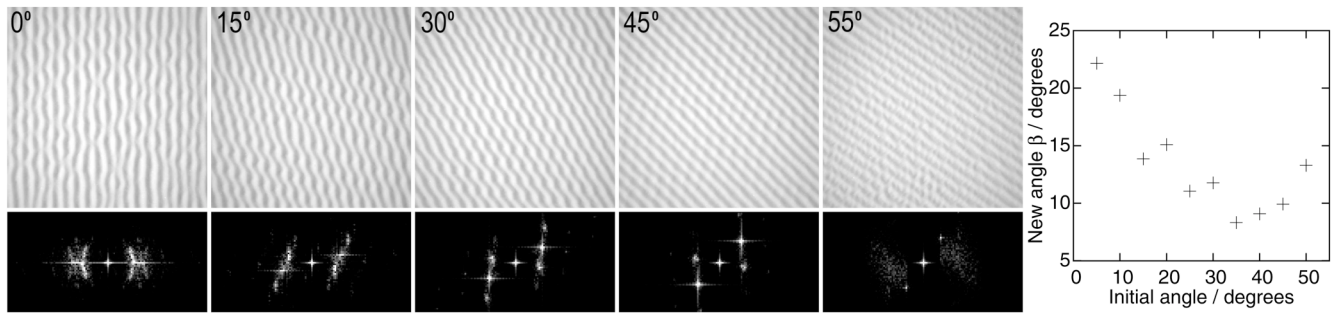
FIG. 5. The same initial pattern subjected to a driving of $a=30$ mm and $f=0.80$ Hz, with varying initial angle $\alpha$, measured after 100 oscillations. For $\alpha$ near 0°, symmetric bulging of the ripples occurs (cf. [4]). At low angles from 10° to around 35°, the bulges are asymmetric. A smooth transition from bulges to superposed ripples exists around $\alpha=35°$, while the superposed ripples vanish at 50°. The angle of the bulges and superposed ripples as a function of the initial angle is plotted in the graph, and a stable area between around 35° and 50° is seen.

With $\alpha$ from around 35° to 50° the transition is more regular. The spots on the FFT corresponding to the thick part of the zigzag become more well defined and less blurred. This means that the pattern is more regular and that the angles of the two parts of the zigzag are more sharply defined. Therefore, it is meaningful to consider the pattern as two superposed ripple patterns with angles $\alpha$ and $\beta$.

No clear distinction can be made between the bulges and the new superposed ripples by looking directly at the ripples or by analyzing the FFT. The transition from one to the other is not very sharp. However, when looking at the graph in Fig. 5 (right), it is clear that the angle $\beta$ of the thick bulges changes with $\alpha$ until around 35° and then stabilizes at an angle of about 8° until $\alpha$ reaches about 50°. At $\alpha=50°$, $\beta$ is higher than when $\alpha$ lies between 35° and 45°, but almost within the uncertainty. The transition dynamics slows down when $\alpha$ is raised, because the ripple profile along the direction of the motion becomes less steep when the ripples are turned, making the shear stress on the bed smaller. The vortex created behind the ripple crest diminishes with increasing angle and eventually vanishes. This agrees with the fact that no superposed ripples are created at 55°. Instead, rolling grain ripples emerge, as from a flat bed. The characteristic clouds in the FFT (stemming from the short ripple distance rolling grain ripples) can be seen at 55° in Fig. 5.

The dynamics observed at $\alpha=55°$ corresponds to qualitative experiments made with water motion parallel to the ripples. In these experiments, rolling grain ripples form in the troughs between the ripple crests. If a grain located on the side of a ripple is dislodged by the shear force, it will move along with the water, parallel to the crest, but also falls sideways toward the bottom of the trough because of the inclination of the ripples. This transversal transport thus leads to the flattening of the original ripples, while the rolling grain ripples in the troughs eventually become real vortex ripples, perpendicular to the water motion, and thereby also to the old ripples.

To summarize this section, superposed ripples with a well-defined angle $\beta$ are found when the angle $\alpha$ is between 35° and 50°. Lowering $\alpha$, a smooth transition between superposed ripples and bulging is found. $\alpha$ above 50° gives no superposed ripples, but leads to the creation of rolling grain ripples in the troughs.

The temporal dynamics of the experiments of this section will be analyzed in Sec. IV, and further indications of the smooth transition around 35° will be presented.

### B. Varying frequency and amplitude

In this part of the experiment, $\lambda$ was held constant at 30 mm, while $\alpha$ was kept at 43° in most experiments, and between 41° and 48° in all. Since $\alpha$ influences $\beta$ much less than $a$ and $f$, the variation in the initial angle causes changes in $\beta$, which are smaller than the intrinsic uncertainty (3°) of the pattern formation.

A simple spline interpolation of all the data points has been chosen to visualize all of the data points shown in Fig. 6. Four data series with different amplitudes are plotted in detail in Fig. 7. A reasonably monotonic behavior is observed for both parameters $a$ and $f$ within this region. The devia-
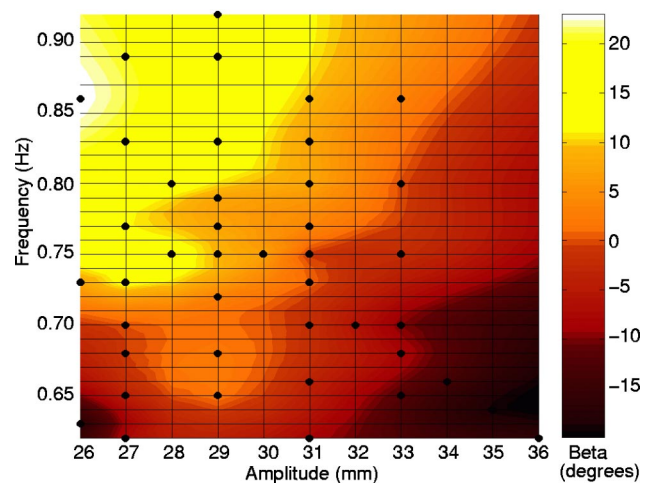


FIG. 6. (Color online) The angle $\beta$ of the superposed ripples at their appearance plotted as a function of frequency and amplitude. The color scheme of the graph originates in a simple spline interpolation of the data points (black dots). It should be considered as an overview of the results only. Both frequency and amplitude influence the angle of $\beta$, in a reasonably simple way. The initial angle $\alpha$ is 43° for most of the data points, and between 41° and 48° for all. The standard deviation of around 3° should be kept in mind.
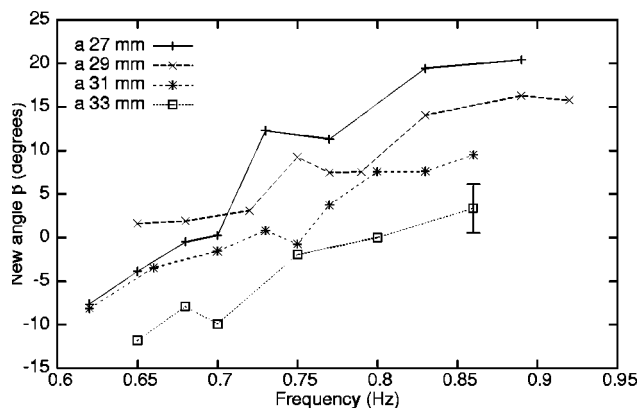
FIG. 7. Part of the data from Fig. 6 plotted in series with constant amplitude. The size of the standard deviation, around 3°, is shown to the right on the graph.

tions from a monotonic behavior are most likely not significant. The limited size of the current data set makes it impossible to say whether a simple plane or a paraboloid is the best fit.

The dynamics curves, described in Sec. IV, remain similar when keeping $af$ constant. Contrary to this, as can be seen from Fig. 6, the angle of the superposed ripples changes most rapidly in the direction where $af$ is constant.

### C. Varying the temperature

As stated in Sec. I, the strong dependence of the superposed angles on the frequency suggests that the phenomenon observed is viscous rather than geometric in origin.

Since the viscosity of water decreases almost by a factor of 2 between 10 and 40 °C, we can change the viscosity easily by changing the temperature. In Fig. 8 the angle $\beta$ is plotted as a function of the temperature. The stars and crosses represent measurements started from initial angles between 35° and 45°, with a fixed frequency ($f=0.77$ Hz)
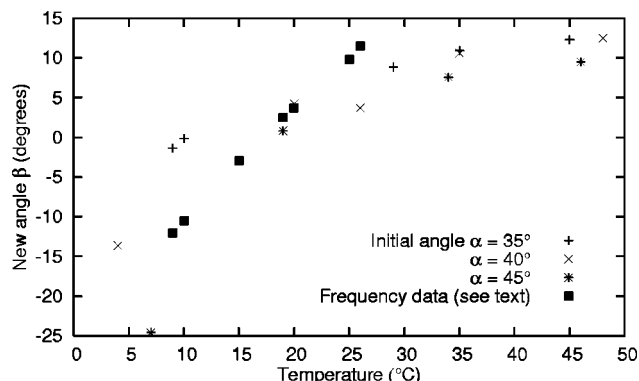


FIG. 8. Measurement of the angle $\beta$ of the superposed ripples as function of the water temperature. All measurements are made at frequency $f=0.77$ Hz and amplitude $a=31$ mm (close to the center of Fig. 6). The different stars represent measurements started from different initial angles $\alpha$: 35°, 40°, and 45°. The black squares show the corresponding variation obtained by using data from Fig. 6 by assuming that $\beta=f(\text{St})$ as explained in the text.

and amplitude ($a=31$ mm). The black squares show the corresponding variation obtained from Fig. 6, with $a=31$ mm and varying frequency. The frequency is converted to the temperature scale assuming that $\beta=f(\text{St})$ and $\text{St}=a^2f/\nu$, and that the measurements of Fig. 6 were performed at $20\pm2$ °C. This means that a change in viscosity (due to the variation in temperature) corresponds to a change in $f$, such that $f/\nu$ remains constant. Although we do see a clear temperature variation in the expected direction in Fig. 8, the variation predicted by this assumption (the black squares) is too rapid, indicating that the effect is not purely hydrodynamical, but that the mobility of the grains (represented, e.g., by the Shields parameter [16] containing the gravitational acceleration) is probably also of importance.

## IV. TEMPORAL EVOLUTION OF THE TRANSITION PROCESS

Most of the experiments with different initial conditions have given the same qualitative features of the transition from the original skewed ripples, through the overlaid pattern, to the new perpendicular ones. What changes is the time scale, meaning the time it takes to reach a specific point in the development of the superposed ripples, for instance, the collapse of the two distinct ripple directions to new, perpendicular ripples.

By the use of *difference pictures*, the overall motion of the ripples can be analyzed, and the dependence of the transition on the frequency and the amplitude can be estimated. The absolute difference between the gray-scale value of a given pixel and the same pixel in the following image is found for the entire picture, so that the areas with large changes in intensity have high values in the difference picture.

A simple measure of the dynamics can be made by counting the number of pixels in the difference picture with a value above some threshold value. This defines a dynamics number $\phi$. For an image size of $512\times512$ pixels, this means that $\phi$ will assume a value between 0 and $512^2$.

When looking at a sequence of images and comparing with the dynamics curves of Fig. 9, some features are noticeable. First a small rise in $\phi$ is observed when the superposed ripples start to emerge. The dynamics decreases again while the superposed ripples grow stronger. They then rise rapidly to the maximum value, which is reached when the superposed ripples start to recombine with neighbors and the defects which were created start to move. In Fig. 2 this corresponds roughly to the fourth image. After the maximum is reached, the dynamics decreases gradually before reaching a stable level. Because of the border effects in the system, movements of the ripples continue at the edges, yielding a higher dynamics number $\phi$ than an infinite system with completely stable ripples would do. When collapsing the curves, by rescaling the two axes for each graph, so that the peak of all curves fall in a single point, a reasonable agreement is seen between the curves (Fig. 9). However, the relaxation of the system does change with frequency.

### A. Variation with initial angle $\alpha$

The smooth transition from bulging to superposed ripples around 35° proposed in Sec. III A is further supported by the
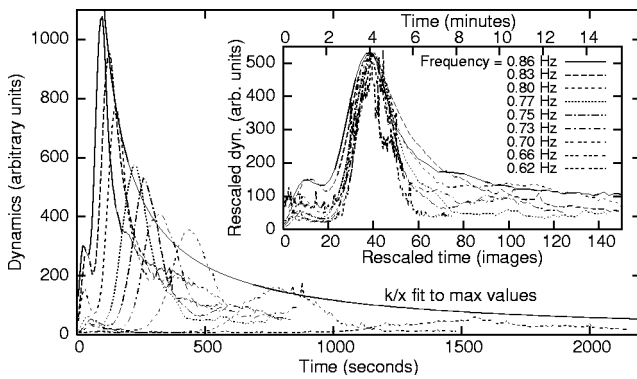
FIG. 9. Dynamics curves from experiments with the same amplitude 31 mm and initial angle 43°, and with different frequencies. The first minor peak after around 50 s corresponds to the emerging of the superposed ripples, while the maximum dynamics is found when the superposed ripples start to recombine with neighbors and create defects. As can be seen, the dynamics depends strongly on the frequency. The maxima of all curves fall on a hyperbola, indicating that the dynamics number $\phi$ multiplied by the time is constant for all experiments. Inset: The same dynamics data collapsed, so that the maxima fall in the same point. It is seen that the curves fall reasonably on top of each other, but that the decay of the dynamics varies with the frequency.

dynamics curves in Fig. 10, generated from the same experiments. At low angles, the bulging of the ripples takes place quite rapidly after the driving of the system has begun. This implies that $\phi$ increases from the beginning and reaches the maximum value, when the bulges recombine with neighbor bulges, and defects are created.

The dynamics at higher initial angles $\alpha$ is different, as described in Sec. III A, with a smaller local dynamic peak in the beginning, when the superposed ripples emerge. The dynamic maximum is reached later, when the superposed ripples recombine with the neighbors. The defects then slowly disappear by recombining, while the dynamics num-
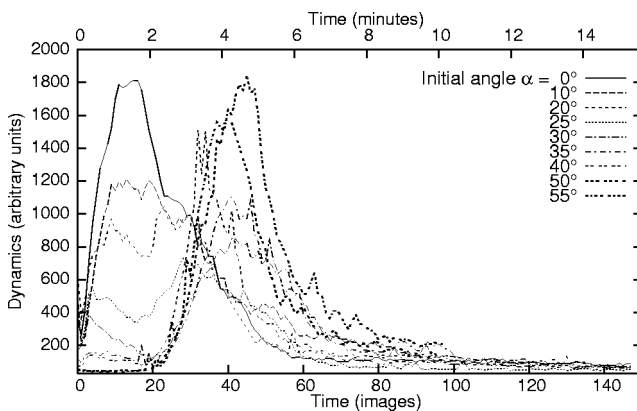


FIG. 10. Dynamics curves for experiments with different angle $\alpha$, and with fixed $a$ and $f$. Two types of behavior are found, corresponding to angles up until 20° (with a rapid initial increase in the dynamics number), and from 35° where the peak is found later. In between, at 25° and 30°, curves with characteristics from both types are found, in agreement with the smooth transition between bulges and superposed ripples which is proposed in Sec. III A.

ber approaches a steady level, in the manner described in Sec. III A.

## V. GRAIN MOTION ON SOLID RIPPLES

### A. Single particle tracking on solid ripples

The angle $\beta$ of the new ripples clearly depends on the driving parameters $f$ and $a$. These parameters influence the way the water moves, and thus the way the sand is moved by the water. Since the original ripples are not perpendicular to the motion of the water, the flow cannot be considered two dimensional, and there must be some net transversal flux during a half period in the direction perpendicular to the water motion (with a flux in the opposite direction during the other half period). In order to visualize this transverse flow and compare it to the geometry and lengths of the sand ripples, a small particle with a density slightly higher than that of water has been used. The movement of the particle can be treated statistically, so that a mean path of the particle can be found. The features of this mean path can then be compared to the geometry of the real sand ripples and a possible connection can be established.

Ideally, the single particle should be tracked on top of the real sand ripples, but since we wish to investigate the angle of the emerging, superposed ripples, data could only be collected during the first few oscillations, before the deformation of the original ripples set in. This deformation alters the flow of the water, and the path of a particle in the water will therefore be changed too.

To overcome these problems, an array of artificial plastic ripples with a ripple distance of 30 mm, corresponding to that of the real sand ripples, was made. The simple geometric profile of the plastic ripples was constructed from an analysis of the shape of real ripples of similar size. The height of the ripples are $40 \times 40$ cm.

A plastic bead with density $\rho$ of 1.2 g/cm$^3$ and a diameter of 2 mm is used as the single tracer particle. The density was thought to be high enough to keep the particle close to the ripples at any time, and close enough to the density of water to give a correct picture of the water motion.

The array of ripples is placed on the tray instead of the sand. The motion of the single particle is recorded from above using a 30 frames per second digital FireWire camera moving with the tray, 10 cm above the lid.

The particle is placed in the middle of the field of view and the motor is started. The particle moves back and forth over the ripple crest, staying on one ripple for a period of time before eventually moving to a neighbor ripple. The motion is not completely periodic, but clearly has some structure, as can be seen in the left graph of Fig. 11.

First, the position of the particle is determined in each image using picture analysis software. Then the mean path of the particle during one oscillation is found by making a floating average, so that the mean position of the particle at a given time is defined as the average of all the positions from one half period before to one half period after the frame. An example of the mean path is seen in Fig. 11(a) on top of the recorded path of the particle. Next, the normalized and temporally averaged path (b) can be calculated. As can be seen
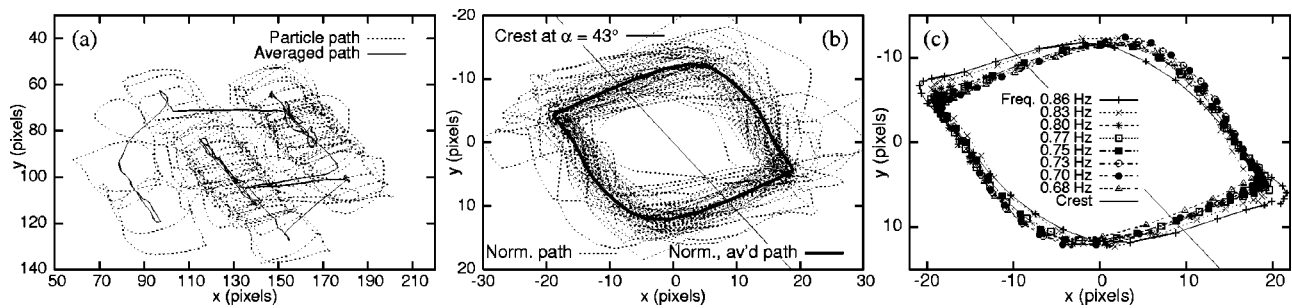
FIG. 11. (a) The particle path, and the particle position averaged over one oscillation. (b) The normalized path is found by subtracting the averaged path from the original path, while the normalized averaged path (solid line) is the temporally averaged normalized path. (c) Normalized averaged paths for different frequencies and the same amplitude 31 mm and initial angle 43°. No apparent differences between the trajectories, which would explain the change in angle $\beta$ of the real superposed ripples with the same parameters, are found.

on the rightmost graph of Fig. 11(c) the paths for different frequencies are almost identical. This is also the case for experiments where $af$ is kept constant. Thus, it is not possible to use these paths to predict the observed changes in the patterns of the superposed sand ripples.

The mean paths displayed in Fig. 11(c) show that the particle is dragged along the ripples almost parallel to the crest until it suddenly jumps across the crest almost orthogonally. The reversal of the stroke then causes a sharp turn of the path before it is dragged back along the other side of the crest, and it clearly illustrates the violent flows created by the separation vortices around the crest [17]. The sudden change from motion along the crest to orthogonal motion is known from streak lines in steady flows across a solid cylinder at a skew angle [18].

### B. Sand on solid ripples

A few qualitative experiments have been performed using a thin layer of sand sprinkled evenly over the plastic ripples. To investigate the importance of the vortex behind the crest, two new sets of artificial ripples with a sinusoidal profile and heights of 6 and 2 mm have been manufactured in aluminum. The ripple distance is 30 mm as that of the plastic ripples.

A regular pattern of superposed ripples can be obtained when the right amount of sand is sprinkled on the plastic ripples [Fig. 12(a)]. If the quantity of sand is too small, no well-ordered structures emerge, while too much sand will make the plastic ripples less important, because the troughs will be filled with sand, effectively creating a different profile. On the 6 mm sine ripples, superposed ripples emerge, but soon develop into perpendicular ripples as seen in Fig. 12(b), presumably because of the weaker vortex behind the crests. No sand ripple formation is observed on the 2 mm ripples, due to the smaller height and the sinusoidal profile.

### VI. SUMMARY AND CONCLUSION

We have investigated the superposed ripples which are created when an array of regular ripples is subjected to a flow nonperpendicular to the crests. It is found that both the driving frequency and the amplitude, as well as the temperature (viscosity), influence the angle $\beta$ of the superposed

ripples, while the initial angle $\alpha$ is of minor importance, when it lies between 35° and 50°. Below 35° the superposed ripples are less well-defined and a smooth transition to asymmetric bulges is found at lower angles. Above 50°, no superposed ripples emerge, presumably because of the reduced slope of the ripple sides in the direction of the flow. Instead rolling grain ripples are created in the troughs.

The temporal evolution of the transition process was quantified and it was shown that the development of the pattern is qualitatively the same for different driving parameters. Furthermore, the smooth transition around $\alpha=30°$, between asymmetric bulges and regular superposed ripples, is supported by the dynamics which shows a similar transition at these angles.

The single particle tracking on solid ripples yielded accurate mean paths with an interesting universal shape reflecting the violent vortex dynamics around the crest, but showing no direct connection with the superposed pattern. On the other hand, a thin layer of sand on an artificial solid ripple-like pattern reproduces the qualitative features of the ripple patterns.

We believe that the origin of the superposed pattern is a centrifugal instability, analogous to the one observed for purely transverse (i.e., nonskewed) ripples [13,19,20], where it creates a brick pattern, similar to the pearling transition
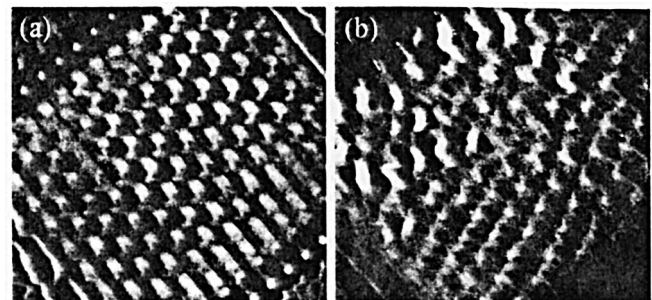


FIG. 12. A thin layer of sand is evenly sprinkled on the solid plastic ripples and oscillated. (a) A pattern of superposed ripples, similar to the ones created in sand, occurs on the ripples with a sharp crest. (b) The superposed ripples are not stable on sine-profile ripples with no sharp crest, but develop into normal perpendicular ripples (left side of image), because the vortex behind the crest is much weaker.

described in [4,10,11]. The basis for this transition is the transverse instability of the flow around an oscillating cylinder [14]. This is supported by the fact that the angle measurements show a clear temperature dependence, which suggests that viscosity plays an important role. These measurements, however, also suggest that the change in the water flow caused by the grain motion is important for the quantitative prediction of the superposed pattern.

---

[1] R. A. Bagnold, Proc. R. Soc. London, Ser. A **187**, 1 (1946).

[2] P. Nielsen, J. Geophys. Res. **86**, 6467 (1981).

[3] A. Brebner, in *17th International Conference on Coastal Engineering*, Sydney, 1980 (American Society of Civil Engineers, New York, 1981), Vol. 2, pp. 1340–1343.

[4] J. L. Hansen, M. van Hecke, C. Ellegaard, K. H. Andersen, T. Bohr, A. Haaning, and T. Sams, Phys. Rev. Lett. **87**, 204301 (2001).

[5] K. H. Andersen, Ph.D. thesis, University of Copenhagen, 1999 (unpublished), available at www.nbi.dk/~kenand

[6] K. H. Andersen, M.-L. Chabanol, and M. van Hecke, Phys. Rev. E **63**, 066308 (2001).

[7] M. A. Scherer, F. Melo, and M. Marder, Phys. Fluids **11**, 58 (1999).

[8] A. Stegner and J. E. Wesfreid, Phys. Rev. E **60**, R3487 (1999).

[9] M. C. Cross and P. C. Hohenberg, Rev. Mod. Phys. **65**, 851 (1993).

[10] J. L. Hansen, Ph.D. thesis, University of Copenhagen, 2001 (unpublished), available at www.nbi.dk/~lundbek

[11] J. L. Hansen, M. van Hecke, A. Haaning, C. Ellegaard, K. H. Andersen, T. Bohr, and T. Sams, Nature (London) **410**, 324 (2001).

[12] E. Siggia and A. Zippelius, Phys. Rev. Lett. **47**, 835 (1981).

[13] T. Hara and C. Mei, J. Fluid Mech. **217**, 1 (1990).

[14] H. Honji, J. Fluid Mech. **107**, 509 (1990).

[15] F. Bundgaard, Master's thesis, University of Copenhagen, 2003 (unpublished), available at www.nbi.dk/~bundgard

[16] J. Fredsøe and R. Deigaard, *Mechanics of Coastal Sediment Transport* (World Scientific, Singapore, 1992).

[17] T. Sand Jespersen, J. Qvist Thomassen, A. Andersen, and T. Bohr, Eur. Phys. J. B **38**, 127 (2004).

[18] M. Sumer and J. Fredsøe, *Hydrodynamics around Cylindrical Structures* (World Scientific, Singapore, 1997).

[19] N. Matsunaga and H. Honji, Rep. Res. Inst. Appl. Mech. (Kyushu Univ.) **28**, 27 (1980).

[20] G. Vittori and P. Blondeaux, J. Fluid Mech. **239**, 23 (1992).